Journal of Zhejiang University-SCIENCE B (Biomedicine & Biotechnology) in press
www.jzus.zju.edu.cn; www.springer.com/journal/11585
E-mail: jzus_b@zju.edu.cn

Research Article

https://doi.org/10.1631/jzus.B2300896

Chronic exposure to hexavalent chromium induces esophageal tumorigenesis via activating the Notch signaling pathway

Yilin ZHU[1], Fanrong LIU[1], Lei LIU[1], Jinfu WANG[1], Fengyuan GAO[1], Lan YE[2], Honglei WU[3], Chengjun ZHOU[4], Guimei LIN[5,6], Xiaogang ZHAO[1,7], Peichao LI[1,7]✉

[1]*Department of Thoracic Surgery, The Second Hospital, Cheeloo College of Medicine, Shandong University, Jinan, Shandong, 250012, China*
[2]*Cancer Center, The Second Hospital, Cheeloo College of Medicine, Shandong University, Jinan, Shandong, 250012, China*
[3]*Department of Gastroenterology, The Second Hospital, Cheeloo College of Medicine, Shandong University, Jinan, Shandong, 250012, China*
[4]*Department of Pathology, The Second Hospital, Cheeloo College of Medicine, Shandong University, Jinan, Shandong, 250012, China*
[5]*Key Laboratory of Chemical Biology (Ministry of Education), School of Pharmaceutical Sciences, Cheeloo College of Medicine, Shandong University, Jinan, Shandong, 250012, China.*
[6]*National Medical Products Administration Key Laboratory for Technology Research and Evaluation of Drug Products, Shandong University, Jinan, 250012, China.*
[7]*Key Laboratory of Chest Cancer, The Second Hospital, Cheeloo College of Medicine, Shandong University, Jinan, 250012, China*

Abstract: Hexavalent chromium [Cr(VI)], as a well-established carcinogen, contributes to tumorigenesis for many human cancers, especially respiratory and digestive tumors. However, the potential function and relevant mechanism of Cr(VI) on the initiation of esophageal carcinogenesis is largely unknown. Here, immortalized human esophageal epithelial cells (HEECs) were induced to be malignantly transformed cells, termed HEEC-Cr(VI) cells, via chronic exposure to Cr(VI), which simulates the progress of esophageal tumorigenesis. In vitro and in vivo experiments demonstrated that HEEC-Cr(VI) cells obtain the ability of anchorage-independent growth, greater proliferative capacity, cancer stem cell properties, and capacity to form subcutaneous xenografts in BALB/c nude mice when compared to its parental cells, HEECs. Additionally, HEEC-Cr(VI) cells exhibited weakened cell motility and enhanced cell adhesion. Interestingly, HEECs with acute exposure to Cr(VI) failed to display those malignant phenotypes of HEEC-Cr(VI) cells, suggesting that Cr(VI)-induced malignant transformation, but not Cr(VI) itself, is the cause for the tumor characteristics of HEEC-Cr(VI) cells. Mechanistically, chronic exposure to Cr(VI) induced abnormal activation of Notch signaling, which is crucial to maintaining the capacity for malignant proliferation and stemness of HEEC-Cr(VI) cells. As expected, DAPT, an inhibitor for the Notch pathway, drastically attenuated cancerous phenotypes of HEEC-Cr(VI) cells. In conclusion, our study clarified the molecular mechanism underlying Cr(VI)-induced esophageal tumorigenesis, which provides novel insights for further basic research and clinical therapeutic strategies about Cr(VI)-associated esophageal cancer.

Key words: Hexavalent chromium [Cr(VI)]; esophageal tumorigenesis; malignant proliferation; stemness; Notch signaling pathway

Unedited

1 Introduction

Esophageal cancer (EC) ranks 7th and 6th in the incidence of human malignant tumors and cancer-related causes of death, respectively, which has been a huge threat to human health (Sung et al., 2021). Esophageal squamous cell carcinoma (ESCC) and esophageal adenocarcinoma (EAC) are two main pathological subtypes that show great variances in their biological characteristics and geographical distribution (Abnet et al., 2018; Morgan et al., 2022). Although current therapy for EC involves chemoradiotherapy, esophagectomy, targeted therapy, and emerging immunotherapies, five-year survival rates of EC patients are approximately 12–20% (An et al., 2023). Among all factors contributing to EC tumorigenesis, environmental pollutants, especially car-

✉ Peichao LI, lipeichao@email.sdu.edu.cn
Peichao LI, https://orcid.org/0009-0003-0126-602X
Yilin ZHU, https://orcid.org/ 0009-0000-5100-5547

Received Dec. 10, 2023; Revision accepted June 17, 2024;
Crosschecked xxx. xx, 20xx; Published online xxx. xx, 20xx

© Zhejiang University Press 2024

cinogenic metal ions, attracted more and more attention and research (Lee et al., 2016; Jiang et al., 2021; Nozadi et al., 2021; Sohrabi et al., 2021).

Hexavalent chromium [Cr(VI)], a well-established carcinogenic metal, is widely distributed in human living environments due to its extensive applications in industrial processes such as plating, stainless steel manufacturing, dyes and pigments, and leather tanning (Iyer et al., 2023). Humans are exposed to Cr(VI) contamination mainly through inhalation, drinking water, and food (Sun et al., 2015). Once entering cells, Cr(VI) is reduced to trivalent [Cr (III)] by glutathione, whereby the production of reactive oxygen species (ROS), formation of Cr-DNA adducts, damage and mutagenesis of the genome, and mitochondrial dysfunction are considered dominant molecular mechanisms underlying Cr(VI) toxicity (Chen et al., 2019). Cr(VI)-induced tumorigenesis has been reported in some murine models and human cells (Islam et al., 2022). For instance, a 2-year study from the National Toxicology Program revealed that chronic oral exposure to Cr(VI) (180 mg/L) through drinking water induced the experimental rats and mice to develop cancer in the oral cavity or the small intestine, respectively (National Toxicology, 2008; Stout et al., 2009). Male A/J mice with inhalation exposure to Cr(VI) developed bronchioloalveolar adenomas and carcinomas in their lungs (Zeidler-Erdely et al., 2020). After long-term exposure (for 20 weeks) to Cr(VI), female C57BL/6J mice formed colorectal cancer and displayed a significant upregulation of proliferative cell nuclear antigen (PCNA) (Zhang et al., 2020). So far, studies exploring the effects of Cr(VI) exposure on human cells have mainly focused on human bronchial epithelial cells (16-HBE and BEAS-2B). For example, studies by Hu et al. revealed that Cr(VI) exposure induced hypermethylation of P16, TP53, and DNA repair genes in 16-HBE cells (Hu et al., 2016; Hu et al., 2018). Sun et al. reported that Cr(VI) exposure-mediated downregulation of HHIP significantly induced the malignant transformation of BEAS-2B cells (Sun et al., 2011; Li et al., 2021a). However, the association between Cr(VI) and esophageal tumorigenesis and its potential molecular mechanisms have not been fully explored.

Notch signaling, as an evolutionarily conserved pathway, deeply participates in the regulation of development, homeostasis, and renewal in multiple tissues and organs (Zhou et al., 2022). When ligand-mediated activation occurs, Notch receptors are cleaved three times to be the active truncation. Then, the truncated Notch protein is translocated into the nucleus to regulate the transcription of downstream target genes (Kopan and Ilagan, 2009). Attributed to the crucial and pleiotropic physiological roles of the Notch pathway, its dysregulation has been reported to be closely associated with the initiation, progression, immunotherapy, and clinical prognoses in various human cancers (Cai et al., 2023; Li et al., 2023). It is worth noting that the activity status and potential function of the Notch signaling pathway in esophageal epithelial cells with chronic exposure to Cr(VI) remain largely unknown.

In the present study, immortalized human esophageal epithelial cells (HEECs) were selected to undergo chronic exposure to Cr(VI) to become malignantly transformed cells, named HEEC-Cr(VI). Compared to their parental cells, HEEC-Cr(VI) cells possess the ability for anchorage-independent growth in soft agar and subcutaneous growth in BALB/c nude mice and show enhanced cellular stemness. Mechanistically, aberrant activation of the Notch signaling induced by chronic exposure to Cr(VI) is essential to maintain the malignant proliferation and stemness in HEEC-Cr(VI) cells. Our results illuminate the molecular mechanism underlying the initiation of EC induced by Cr(VI), which provides important evidence and promising insights for further studies and treatment strategies about Cr(VI)-associated EC.

2 Materials and methods

2.1 Cell culture

Human esophageal epithelial cells (HEECs), also known as HEsEpiCs, were isolated from the human esophagus in the ScienCell Research Laboratories. Detailed information about HEECs can be found at (https://sciencellonline.com/human-esophageal-epithelial-cells). HEECs were purchased from the BeNa Culture Collection (Beijing, China) and authenticated by Short Tandem Repeat analysis with Tsingke Biotechnology (Beijing, China). DMEM medium (Corning, 10-013-CVRC) supplemented with 1% penicillin/streptomycin (PS) (New Cell & Molecular Biotech, C125C5) and 10% fetal bovine serum (FBS) (ExCell Bio, FSP500) was applied for cell culturing. All cells were grown in an incubator with 5% CO_2 at 37 °C.

Unedited

2.2 Establishment of transformed cells induced by Cr(VI)

HEECs were cultured in the complete medium (DMEM supplemented with 10% FBS and 1% PS) containing 0.25 μM or 0.5 μM of Cr(VI). When the confluence of cultured cells was approximately 90%, the cell passaging was performed. It should be noted that the limited expansion capacity of HEECs restricts their long-term cultures according to information from the ScienCell Research Laboratories. The potassium chromate (CrK_2O_4) (Sigma-Aldrich, 216615) was applied for Cr(VI) exposure. Interestingly, HEECs with ongoing exposure to Cr(VI) (0.25 μM) displayed an increasingly strong capability for amplification. However, after a few weeks of exposure to Cr(VI) (0.5 μM), HEECs failed to maintain enough viability for the passaging. Every 10 generations, the soft agar colony formation assay was applied to evaluate the anchorage-independent growth of HEECs with chronic Cr(VI) exposure. Finally, after 60 generations of exposure to Cr(VI) (0.25 μM), the transformed HEEC cell line possessed the significant capacity to anchorage-independently grow in the soft agar and was named HEEC-Cr(VI).

2.3 Mice and xenograft models

BALB/c athymic nude mice (4 weeks old; male) were obtained from Beijing Vital River Laboratory Animal Technology Co., Ltd. (Beijing, China). Mice were housed in a ventilated cage with 12/12 hours of a light/dark cycle, a temperature between 18°C and 23 °C, and 40–60% relative humidity. To establish xenograft models, each nude mouse was subcutaneously injected with 5×10^6 cells in the axillary fossa. Tumor sizes were measured every 4 days and calculated with the following formula: (longest-diameter × shortest-diameter^2)/2. The mice were euthanized when the maximum volume of xenografts reached or exceeded 1000 mm^3.

2.4 Soft agar colony formation assay

Cells were suspended in culture medium supplemented with 1% PS, 10% FBS, and 0.35% low-melting-point agarose (Sigma, A4018) and were then added into 6-well plates with medium containing 0.5% low-melting-point agarose on the bottom for 3 weeks. Detailed procedures and the counting method were described in our previous study (Li, et al., 2021a).

2.5 EdU incorporation assay

A total of 5×10^3 cells were cultured into one well in a 96-well plate for 24 hours. The BeyoClick™ EdU-594 kit (Beyotime, C0078S) was applied for the assay. After the culture medium was discarded, 100 μL of 5-ethynyl-2-deoxyuridine solution was added into each well for 2 hours of incubation. Then, 4% paraformaldehyde was utilized to fix the cells. After being washed with 3% bovine serum albumin (BSA) and permeabilized by 0.3% Triton X-100, the cells were incubated with Click Reaction Buffer for 30 minutes followed by nuclear staining with 1 × Hoechst 33342 reaction solution. Images were captured using a fluorescence microscope. The percentage of EdU-positive cells was calculated using the following formula: (EdU-stained cells/Hoechst-stained cells) ×100%. The assay was performed in three replicate wells.

2.6 Cell viability assay

A total of 3×10^3 cells were seeded into each well of a 96-well plate. Then, 10 μL of CCK-8 reagent (Solarbio, Beijing) was added into each well on days 0, 1, 2, and 3, respectively. After 2 hours of incubation, the absorbance at 450 nm was measured by using an Infinite M200 PRO NanoQuant microplate reader (TECAN, Switzerland). The mean value of absorbance was calculated from three replicate wells.

2.7 Plate colony formation assay

Cells (1,000/well) were cultured in a 6-well plate for about 2 weeks with a change of medium every 3 days. Then, the colonies underwent fixation with 4% paraformaldehyde and staining with 0.1% crystal violet. The following formula was applied to estimate the rate of plate colony formation: (colonies number/1,000)×100%.

2.8 Sphere formation assay

Single-cell suspension was prepared in serum-free DMEM/F12 medium (Gibco, C11330500BT) supplemented with 20 ng/mL epidermal growth factor (MCE, HY-P7109) and 10 ng/mL basic fibroblast growth factor (MCE, HY-P7004). The cells were then plated in ultra-low attachment 6-well plates (Corning, 3471) at a density of 2,000 cells/well. The plates were gently settled in an incubator for 2 weeks. Speres more than 75 μm were

Unedited

counted and the following formula was applied to calculate the rate of sphere formation: (sphere number/2,000)×100%.

2.9 Wound healing assay

Cells were seeded in 6-well plates and were grown to confluence. A standardized wound was introduced by scratching the monolayer with a sterile 200 μL pipette tip. After scratching, cells were washed with PBS and captured using a microscope with the MShot Image Analysis System (MShot, Guangzhou, China). Then, a medium containing 1% serum was added to each well. After 24 hours of incubation, wound images were captured to document the closure rate. The relative closure rate was calculated by the formula: 100% − (wound area after 24 hours/initial wound area) × 100%.

2.10 Transwell assay

Transwell chambers (Corning, 3422) with uncoated upper surfaces or those precoated with BD Matrigel Matrix (BD Biosciences, 356234) were used for the migration and invasion assays, respectively. Cell suspension (4×10^4 cells into 200 μL serum-free DMEM) was planted on the upper surface of the chamber. Then, the chamber was placed into a 24-well plate with each well containing 600 μL of DMEM medium with 10% FBS for 48 hours. The cells were fixed in 4% paraformaldehyde for 15 minutes, permeabilized by methanol for 15 minutes, then stained with 0.1% crystal violet overnight. After removing non-migrating or non-invading cells, the staining images were captured using a microscope with the MShot Image Analysis System (MShot, Guangzhou, China). Three random fields of each chamber were selected to quantify the migrating or invading cells.

2.11 Reverse transcription-quantitative polymerase chain reaction (RT-qPCR)

Total RNA from cultured cells was extracted using RNA-Quick Purification Kit (Shanghai Yishan Biotechnology, RN001) following the instructions and then subject to concentration detection using the NanoDrop 2000 spectrophotometer (Thermo Fisher Scientific, USA). Extracted RNA (1 μg) was utilized to synthesize cDNA using the LunaScript™ RT SuperMix Kit (NEB, E3010). Then, qPCR was carried out using the Power SYBR® Green Master Mix (Thermo Fisher Scientific, 4367659) on a QuantStudio™ 5 System (Thermo Fisher Scientific). GAPDH mRNA expression was detected as the internal control. The analytic method of $2^{-\Delta\Delta CT}$ was applied to calculate the relative mRNA levels of target genes. Detailed information about primer sequences is summarized in Supplementary Table 1.

Unedited

2.12 Western blot analysis

Total proteins from cells were harvested with the lysis buffer consisting of 10 mM of Tris-HCl (pH 7.4), 1% of SDS, and 1 mM of Na_3VO_4. Then, the concentration of extracted protein was measured using a NanoDrop 2000 spectrophotometer (Thermo Fisher Scientific). For the extraction of cytoplasmic and nuclear proteins, the Minute™ Cytoplasmic and Nuclear Extraction Kit (Invent, SC-003) was applied to lyse cells according to the instructions, followed by concentration measurement via the BCA protein assay kit (NCM Biotech, WB6501). Equivalent amounts of cell proteins were separated using SDS-PAGE and then transported to nitrocellulose membranes (Merck Millipore, HATF00010). After being blocked in tris-buffered saline (TBS) with 5% skim milk, the membranes were washed three times in TBS and incubated with primary antibodies at 4°C overnight, followed by incubation with corresponding secondary antibodies for 1 hour at room temperature. The signals from target proteins were detected using an ECL system (Millipore, WBKLS0500) and the Tanon Imaging System (Tanon, China). The protein levels from three independent experiments were quantified using the Image J software (Schneider et al., 2012). Antibodies used here are listed in Supplementary Table 2. The full and uncropped western blots were present in the Supplementary data.

2.13 Immunofluorescence (IF) assay

A total of 150,000 cells suspended in 3 mL of medium were added into the Glass Bottom Cell Culture Dish (Biosharp, BS-15-GJM) to grow for 24 hours. Then, the cells were fixed with 4% paraformaldehyde for 10 minutes, permeabilized by 0.3% Triton X-100 for 10 min and blocked by 5% BSA for 1 hour. The cells were incubated with indicated primary antibodies at 4°C overnight followed by corresponding fluorescence-conjugated secondary antibodies. After the treatment with an antifade mountant containing DAPI (So-

larbio, S2110), images were captured by a confocal laser-scanning microscope (LSM 800, Zeiss, Germany). The antibodies used for IF are summarized in Supplementary Table 2.

2.14 RNA sequencing

Total RNAs from HEECs or HEEC-Cr(VI) cells were extracted from three duplicate wells in 6-well plates with Trizol universal agent (Tiangen, DP424) and sent to Novogene (Beijing, China) for RNA sequencing. RNA qualification was detected using the Bioanalyzer 2100 system (Agilent Technologies, CA, USA). After constructing libraries with the NEBNext® Ultra™ RNA Library Prep Kit for Illumina® (NEB, E7530), we performed sequencing with the Illumina NovaSeq 6000 (Illumina, USA) following the 150 bp paired-end strategy. Paired-end clean reads obtained from raw data (FASTQ sequence files) were aligned to the Homo Sapiens (GRCh38/hg38) by using HISAT2 (v2.0.5). Gene expression levels were normalized as fragments per kilobase of transcript per million base pairs sequenced. DESeq2 R package (1.16.1) was adopted to analyze the differentially expressed genes (DEGs) between HEEC-Cr(VI) and HEEC groups with the criteria of $|\log2(\text{foldchange})| > 1$ and adjusted P value < 0.05. The gene ontology (GO) analysis of the DEGs was plotted using an online platform (https://www.bioinformatics.com.cn) (last accessed on 10 Nov 2023) for data analysis and visualization (Tang et al., 2023). Gene set enrichment analysis (GSEA) was performed using GSEA software (Subramanian et al., 2005).

2.15 Statistical analysis

Statistical analyses were conducted using the Prism software version 8.0.1 (GraphPad, USA). All experiments were performed independently at least three times unless noted. The two-way analysis of variance (ANOVA) test was performed for the statistical analyses of cell vitality assays and growth curves of xenograft tumors, while other differences between any two groups were determined using the paired or unpaired *t*-test. Measurement data are presented as the mean ± SD. When the P value is less than 0.05, differences are considered significant.

Unedited

3 Results

3.1 HEECs with chronic exposure to Cr(VI) acquire the phenotypes of malignant proliferation and stemness

As shown in Fig. 1a, the IC_{50} value of Cr(VI) for 24 or 48 hours of treatment is 7.198 μM or 4.208 μM in HEECs. To explore the potential effects of chronic exposure to Cr(VI) on the initiation of esophageal cancer, we continuously cultured HEECs in the medium with 0.25 μM of Cr(VI) for 60 generations for approximately 6 months and then obtained the transformed cell line, named HEEC-Cr(VI) (Fig. 1b). The anchorage-independent growth in soft agar has been considered a key phenomenon for the malignant transformation of normal cells (Freedman and Shin, 1974; Shin et al., 1975). Our results revealed that HEEC-Cr(VI) cells formed obvious colonies in soft agar while HEECs can hardly proliferate under the same conditions (Fig. 1c), which suggests that HEEC-Cr(VI) cells are derived from the malignant transformation of their parental cells. To determine the proliferative capacity of HEEC-Cr(VI) cells, we performed the assays of EdU incorporation, CCK-8, and plate colony formation. Our results demonstrated an enhanced proliferation of HEEC-Cr(VI) cells when compared to HEECs (Figs. 1d-f). The acquisition of malignantly proliferative potential is usually accompanied by an increase in cell stemness (Aponte and Caicedo, 2017; Jing et al., 2021). As expected, a sphere formation assay revealed a significantly enhanced stemness in HEEC-Cr(VI) cells (Fig. 1g), which was further supported by increased protein levels of c-Myc and SOX-2, markers for cell stemness (Figs. 1h and S1a, b). To evaluate the tumorigenicity of HEEC-Cr(VI) cells in vivo, subcutaneous formation of xenograft in BALB/c nude mice was performed. Consistent with the phenotypes in vitro, HEEC-Cr(VI) cells, but not their parental cells (HEECs), displayed a significant ability to xenograft subcutaneously (Figs. 1i-k). Together, these results suggest that chronic exposure to Cr(VI) induced HEECs to acquire malignantly proliferative capacity and stemness.

3.2 HEEC-Cr(VI) cells display attenuated cell motility and enhanced cell adhesion

To explore the cellular motility of HEEC-Cr(VI), we conducted wound healing assays and found the migration capacity of HEEC-Cr(VI) cells was weakened compared to HEECs (Fig. 2a). Similarly, transwell assays

revealed that the migration and invasion of HEEC-Cr(VI) cells were attenuated compared with HEECs (Fig. 2b). Additionally, when digested by trypsin, HEEC-Cr(VI) cells took more time to detach from the culture dish compared to HEECs (Fig. 2c). In line with the weakened cell migration and invasion, HEEC-Cr(VI) cells exhibited an increased level of E-Cadherin and a reduced MMP-2 protein expression when compared to HEECs (Figs. 2d and S2a, b). However, we did not observe distinct differences in the morphology of the two types of cells (Fig. 2e). Collectively, HEEC-Cr(VI) cells possess the characteristics of weaker cell motility and stronger cell adhesion compared to their parental cells.

3.3 Acute exposure to Cr(VI) failed to confer HEECs with the characteristics of HEEC-Cr(VI) cells

To determine whether the phenotypes of malignant proliferation and stemness in HEEC-Cr(VI) cells are from the transformation induced by Cr(VI) chronic exposure or from Cr(VI) itself, HEECs were treated with 0.25 μM of Cr(VI) for 48 hours. Our results demonstrated that HEECs with acute treatment of Cr(VI) failed to form colonies in soft agar (Fig. 3a). Similarly, EdU incorporation and CCK-8 assays revealed no prominent difference in proliferative capacity in HEECs between acute exposure to Cr(VI) and vehicle control groups (Figs. 3b, c), while plate colony formation assays displayed a reduced number of colonies from HEECs with acute exposure to Cr(VI) (Fig. 3d). Interestingly, although acute exposure to Cr(VI) had no effects on the stemness of HEECs, the protein levels of c-Myc and SOX-2 displayed a slight decrease upon the treatment of Cr(VI) for 48 hours (Figs. 3e, f and S3a, b). In addition, wound healing and transwell assays revealed that acute exposure to Cr(VI) displayed no alteration in the motility of HEECs (Fig. 3g, h). Consistently, there was no change in protein levels of E-Cadherin and MMP-2 upon 48 hours of exposure to Cr(VI) (Figs. 3i and S3c, d). Together, these results support the suggestion that the biological characteristics, especially the malignant proliferation and stemness, of HEEC-Cr(VI) cells are derived from Cr(VI)-induced transformation but not from Cr(VI) itself.

3.4 Notch signaling pathway is abnormally activated in HEEC-Cr(VI) cells

To explore potential mechanisms responsible for HEECs' malignant transformation induced by chronic exposure to Cr(VI), we applied RNA-Seq to obtain gene expression profiles from HEEC-Cr(VI) and HEECs. As shown in Fig. 4a, when compared to HEECs, a total of 2,381 DEGs (1,447 upregulated and 934 downregulated genes) were identified in HEEC-Cr(VI) cells following the conditions of adjusted P value < 0.05 and |log2(fold change)| > 1. The GO analysis based on upregulated DEGs revealed the association with the terms of epidermis development and transcriptional activity, while downregulated DEGs showed a close correlation to the extracellular matrix and cell migration (Figs. S4a, b), which is consistent with the enhanced proliferation and attenuated mobility of HEEC-Cr(VI) cells. Since HEEC-Cr(VI) cells acquired malignant proliferation and stemness, we further analyzed the related signaling pathways, including Wnt, Hedgehog, and Notch. GSEA results revealed abnormal activation of the Notch signaling pathway, an obvious inhibition of the Wnt signaling, and no significant alterations of the Hedgehog pathway in HEEC-Cr(VI) (Fig. 4b and Figs. S5a, b). To verify the results from RNA-Seq, we performed RT-qPCR to detect the mRNA levels of the Notch signaling ligands (JAG1 and JAG2), receptor (NOTCH3), and downstream target (HES4), and determined their upregulation at the mRNA level in HEEC-Cr(VI) cells (Fig. 4c). Similarly, upregulated JAG1 and JAG2 protein levels and increased nucleus accumulation of active truncate of NOTCH3 protein (NICD3) were found in HEEC-Cr(VI) cells (Figs. 4d, e and S6a-c). Additionally, IF assays revealed the increased JAG2 and NOTCH3 proteins in cell membranes and the accumulation of nucleus NICD3 protein in HEEC-Cr(VI) cells (Figs. 4f, g). These results confirm the aberrant activation of the Notch signaling in HEEC-Cr(VI) cells. Interestingly, bioinformatics analysis based on GEO datasets (GSE130078) (You et al., 2019) and the TCGA database from the UCSC Xeno platform (Goldman et al., 2020) showed that mRNA levels of components in the Notch pathway are upregulated in ESCC (Figs. S7a-e), which further supports the potentially key role of the Notch signaling during Cr(VI)-induced malignant transformation of HEECs.

To rule out the possibility that the activated Notch signaling pathway is directly caused by Cr(VI) itself, HEECs were exposed to 0.25 μM of Cr(VI) for 48 hours and were then subject to the detection of JAG1, JAG2, NOTCH3, and HES4 expression levels. As shown in Fig. 4h, JAG1, JAG2, and HES4 mRNA levels showed no obvious alteration in HEECs upon acute exposure to Cr(VI), while NOTCH3 was significantly decreased. Consistently, the treatment of Cr(VI) (0.25 μM) for 48 hours did not affect protein levels of JAG1 and JAG2 (Figs. 4i and S8a, b). It should be noted that nucleus accumulation of NICD3 protein was not altered in HEECs upon acute exposure to Cr(VI) (0.25 μM) (Fig. 4j and S8c). Taken together, these results indicate that aberrant

Unedited

activation of the Notch signaling pathway is the property of HEEC-Cr(VI) cells but not the consequence directly caused by Cr(VI).

3.5 Blockage of the Notch signaling pathway impairs the malignant proliferation and stemness of HEEC-Cr(VI) cells

To identify the function of the Notch signaling pathway in the malignant phenotypes of HEEC-Cr(VI) cells, DAPT, a potent inhibitor against the Notch signaling pathway, was applied. Unsurprisingly, DAPT treatment not only decreased NICD3 protein levels in the nucleus but downregulated HES4 mRNA expression in HEEC-Cr(VI) cells (Figs. 5a, b and S9a). Then, we evaluated the malignantly proliferative capacity of HEEC-Cr(VI) cells treated with DAPT or vehicle control. Interestingly, DAPT treatment remarkedly diminished the anchorage-independent growth of HEEC-Cr(VI) cells in soft agar (Fig. 5c). In addition, DAPT-induced inhibition on malignant proliferation of HEEC-Cr(VI) cells was further confirmed by reduced EdU incorporation, attenuated cell viability, and impaired formation of plate colonies (Figs. 5d-f). Similarly, sphere formation assays revealed that the stemness of HEEC-Cr(VI) cells was significantly impaired by DAPT treatment (Fig. 5g). Further detection on c-Myc and SOX-2 proteins demonstrated that DAPT treatment markedly downregulated c-Myc expression but had no effect on SOX-2 protein levels (Figs. 5h and S9b, c), which indicates that other pathways are involved in SOX-2 upregulation in HEEC-Cr(VI) cells. In addition, we explored whether the activated Notch signaling pathway regulates the weakened mobility of HEEC-Cr(VI) cells. Wound healing and transwell assays revealed that the migration and invasion of HEEC-Cr(VI) cells were not altered by DAPT (Figs. 5i, j). Conformably, DAPT treatment did not affect E-Cadherin and MMP-2 protein levels (Figs. 5k and S9d, e). Collectively, these results suggest that the activation of the Notch signaling pathway is essential to maintain the malignant proliferation and stemness in HEEC-Cr(VI) cells.

Unedited

4 Discussion

Cr(VI) contaminations via inhalation, drinking water, and food are deeply associated with the morbidity of many human cancers, which pose a huge threat to human health (Sun, et al., 2015; Chen, et al., 2019; Iyer, et al., 2023). However, the exact function of Cr(VI) in esophageal tumorigenesis and the molecular mechanism underlying the initiation of Cr(VI)-associated EC remain largely unknown. Here, we found that HEECs with long-term exposure to Cr(VI) obtained the capability of anchorage-independent growth in soft agar and subcutaneous xenograft in BALB/c nude mice as well as stemness, among which, abnormally activated Notch signaling induced by chronic exposure to Cr(VI) is responsible for the maintenance of malignant proliferation and stemness in HEEC-Cr(VI) cells (Fig. 6).

To determine the function of chronic exposure to Cr(VI) in the occurrence of EC, HEECs were continuously cultured in the medium with Cr(VI) (0.25 μM) for approximately 6 months to establish the transformed cell line, HEEC-Cr(VI). The in vitro and in vivo experiments demonstrated that HEEC-Cr(VI) cells can anchorage-independently grow in soft agar and subcutaneously xenograft in BALB/c nude mice, which suggests Cr(VI)-induced malignant transformation of HEECs. Interestingly, HEEC-Cr(VI) cells exhibit enhanced cell adhesion and attenuated cell motility compared to their parental cells, HEEC, which was further supported by upregulated E-Cadherin and downregulated MMP-2 in HEEC-Cr(VI) cells. Consistent with our finding, the study by Hong et al. reported that genes related to cell junction are significantly increased in Cr(VI)-induced transformed BEAS-2B cells (Sun, et al., 2011). It is noteworthy that altered E-Cadherin protein levels usually indicate epithelial-mesenchymal transition (EMT) (Brabletz et al., 2021). However, no obvious differences in morphology were found in HEEC-Cr(VI) cells. Some studies have reported that chromium exposure is closely associated with the incidence of ESCC (Amer et al., 1990; Hashemian et al., 2017). Interestingly, HEEC-Cr(VI) cells display increased expression of SOX-2, a marker related to squamous cell carcinoma (Hsieh et al., 2019), compared to HEECs. In summary, these results demonstrated that HEECs possess malignantly proliferative capacity after chronic exposure to Cr(VI). It should be pointed out that introducing another cell line for the establishment of Cr(VI)-induced transformed cells in our further study may help to identify the HEEC-specific phenotypes, although HEECs were recommended as an excellent model for the study of esophageal carcinogenesis (https://sciencellonline.com/human-esophageal-epithelial-cells).

To rule out the possibility that Cr(VI) itself directly enhances the malignant proliferation, we treated HEECs

with 0.25 μM of Cr(VI) for 48 hours. The soft agar colony formation assay revealed that HEECs with acute exposure to Cr(VI) failed to develop colonies in soft agar. Additionally, CCK-8, EdU incorporation, sphere formation, and transwell assays demonstrated that acute exposure to Cr(VI) had no effects on HEEC proliferation, stemness, or motility. These results further confirmed that it is Cr(VI)-induced transformation, not Cr(VI) itself, that confers the property of malignant proliferation to HEECs. Interestingly, the study by Fei et al. found that 24 and 48 hours of exposure to Cr(VI) (0.4 μM) promoted the proliferation, migration, and invasion of bladder cancer cells by regulating FLNA (Sheng et al., 2021). Another study from the same research team revealed that acute exposure to Cr(VI) enhanced the migration of prostate cancer cells by promoting EMT (Zhang et al., 2019). Together, these findings indicate that the impact of short-term exposure to Cr(VI) on proliferation and EMT is different between normal epithelial cells and cancer cells.

In an attempt to clarify the mechanism by which Cr(VI)-induced malignant proliferation of HEECs, RNA-seq analysis was performed in HEECs and HEEC-Cr(VI) cells to obtain the profile of DEGs. Further exploration based on GSEA identified abnormal activation of the Notch signaling pathway. Notch signaling is an evolutionarily conserved pathway that is closely associated with the development process, physiological homeostasis, and tissue renewal (Zhou, et al., 2022). It has been reported that Notch signaling regulates the development of the esophageal squamous epithelium in the normal esophagus and acts as a tumor suppressor pathway to inhibit esophagus tumorigenesis induced by 4-nitroquinoline 1-oxide (Sawangarun et al., 2018). However, the dysregulation of the Notch signaling functions with a dual role, an oncogenic or a tumor suppressor pathway, in esophagus carcinogenesis, which is totally dependent on the specific cellular and genetic context (Ranganathan et al., 2011; Sun et al., 2014; Zhong et al., 2015; Nowell and Radtke, 2017; Li et al., 2021b). In the present study, to confirm the function of abnormally activated Notch signaling in the malignant proliferation of HEEC-Cr(VI), we performed the blocking experiments by applying DAPT, an inhibitor against the Notch signaling pathway, and determined its essential role in maintaining a tumor-like proliferative capacity. Remarkably, Natsuizaka et al. reported that activated Notch signaling in ESCC accelerates EMT and tumor initiation via increasing cancer stem cells (Natsuizaka et al., 2017), while our study found that the activation of the Notch pathway and enhanced stemness in HEEC-Cr(VI) cells were accompanied by increased E-Cadherin expression. Additionally, DAPT treatment failed to affect E-Cadherin and MMP-2 expression in HEEC-Cr(VI) cells, suggesting that Notch signaling is not involved in regulating EMT during Cr(VI)-induced malignant transformation of HEECs.

According to the guideline value from the World Health Organization (WHO), total chromium in drinking water should not exceed 50 μg/L (2022). Some regions have set stricter restrictions for Cr(VI) in drinking water, such as a limit of 10 μg/L in California or 5 μg/L in Italy (Chrysochoou et al., 2016). However, the Cr(VI) concentration in the groundwater of some regions with ultramafic rocks has been reported to be between 0.2 and 180 μg/L (Chrysochoou, et al., 2016). For example, In La Spezia (Italy), the concentration of Cr(VI) in the groundwater reached 73 μg/L, significantly exceeding the limitation of 5 μg/L (Fantoni et al., 2002). In our study, the applied concentration of potassium chromate (CrK_2O_4) (Sigma-Aldrich, 216615) is 0.25 μM, equivalent to 13 μg/L of total chromium, which is lower than the guideline value from WHO and the Cr(VI) concentration in groundwater of some ultramafic regions. It is worth noting that one study focusing on arsenic and chromium topsoil levels revealed an association between chromium concentration in topsoil and women's esophageal cancer mortality in Spain (Nunez et al., 2016). Furthermore, a case-control study by Nozadi et al. reported that chromium concentrations (8.1 ± 7.31 μg/kg) of esophageal cancer from Eastern Iraq, an area with heavy metal pollution, displayed a notable rise compared to non-cancerous tissues (1.98 ± 0.8 μg/kg) (Nozadi, et al., 2021). If assuming tissue density to be approximately 1 kg/dm³, the concentration (8.1 ± 7.31 μg/kg) could be considered 8.1 ± 7.31 μg/L, which is very close to the exposure dose of Cr(VI) (0.25μM or 13 μg/L) used in our study. Given that we have demonstrated the capacity of chronic Cr(VI) (0.25μM) exposure to induce malignant transformation of human esophageal epithelial cells, this study provides a crucial reference for future exploration related to cancer initiation or public health, which will raise more and broader attention to chromium contamination.

5 Conclusions

As a summary, we demonstrated the driving role of chronic exposure to Cr(VI) in esophagus tumorigenesis and clarified the relevant mechanism by which Cr(VI)-induced activation of the Notch signaling contributes to

Unedited

the malignant proliferation and stemness of HEEC-Cr(VI) cells. Our study provides a novel potential target for clinical therapy of Cr(VI)-related esophageal tumors.

Data availability statement

All data about this study are present in the article and/or Supplementary data.

Acknowledgments

This study was financially supported by grants from the Special Construction Project Fund for Taishan Mountain Scholars of Shandong Province (to Xiaogang ZHAO), the Jinan Medicine Research Program (to Xiaogang ZHAO), the Nurturing and Development Fund from The Second Hospital of Shandong University (2022YP62) (to Peichao LI), and the Shandong Provincial Natural Science Foundation for Young Scholars (ZR2022QH285) (to Peichao LI).

Author contributions

Peichao LI and Xiaogang ZHAO contributed to the conception and design of this project. Yilin ZHU performed most of the experiments and data analysis. Fanrong LIU, Lei LIU, Jinfu WANG, and Fengyuan GAO assisted with bench work. Lan YE, Honglei WU, and Chengjun ZHOU provided technical assistance for animal experiments. Peichao LI and Yilin ZHU wrote this manuscript. Guimei LIN and Xiaogang ZHAO revised this manuscript. Peichao LI supervised the processes of this project. All authors have reviewed and approved the final manuscript, and therefore, have full access to all the data in the study and take responsibility for the integrity and security of the data.

Compliance with ethics guidelines

Yilin ZHU, Fanrong LIU, Lei LIU, Jinfu WANG, Fengyuan GAO, Lan YE, Honglei WU, Chengjun ZHOU, Guimei LIN, Xiaogang ZHAO, and Peichao LI declare that they have no conflict of interest.

All experiments involved in mice were conducted in the Animal Research Center of The Second Hospital of Shandong University and approved by the Ethical Committee for Animal Experimentation of The Second Hospital of Shandong University (No. KYLL-2022A195).

Unedited

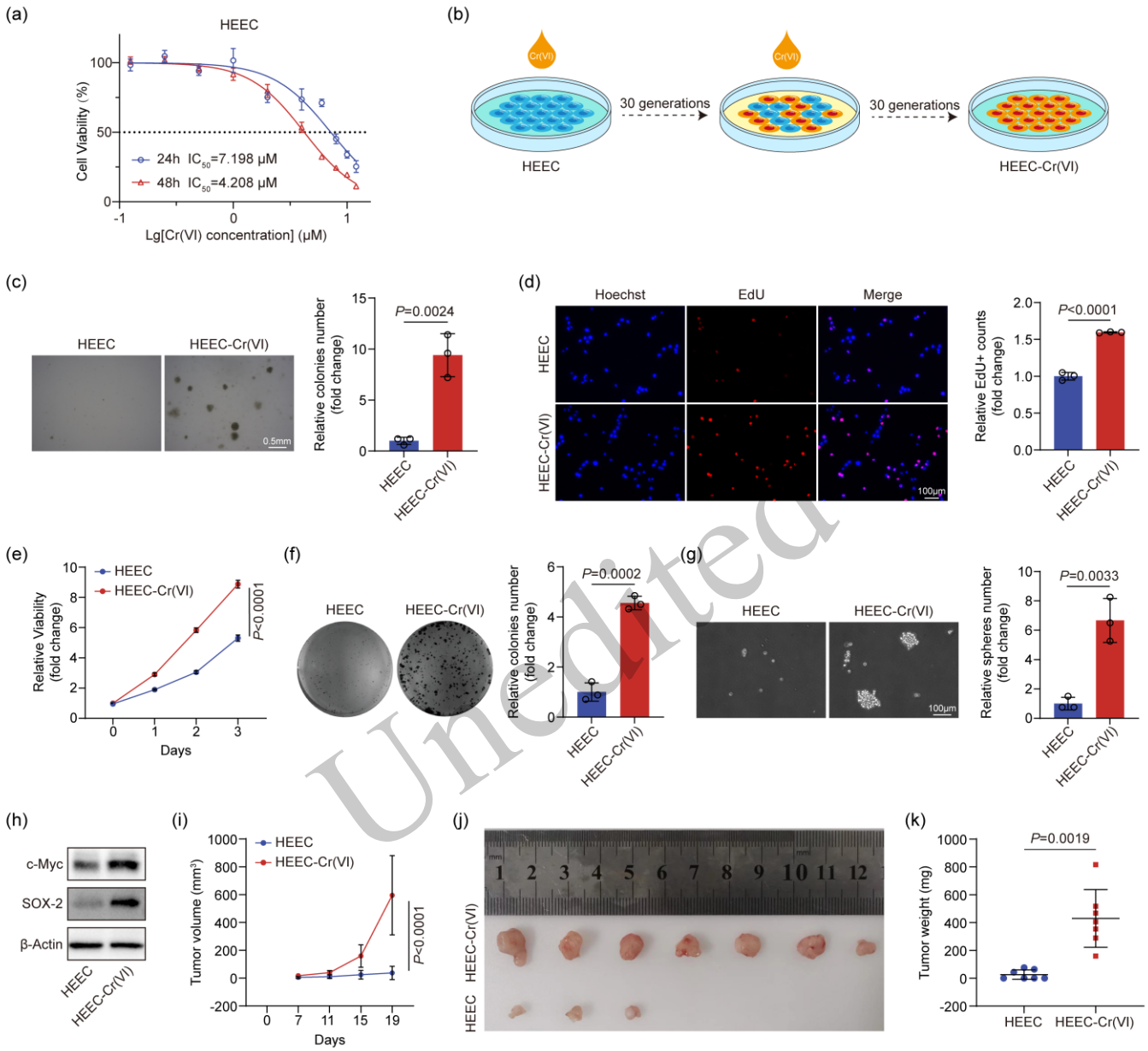

Unedited

Fig.1. HEECs with chronic exposure to Cr(VI) acquire the ability to malignantly proliferate in vitro and in vivo.
(a) HEECs were treated with different doses of Cr(VI) for 24 or 48 hours and then subjected to cell viability detection via CCK-8 assays. The fitting curves were performed to calculate and plot the IC_{50} values. (b) Schematic diagram clarifying the establishment of Cr(VI)-induced malignant transformed HEECs, named HEEC-Cr(VI). (c) A soft agar colony formation assay was applied to evaluate the anchorage-independent growth of HEECs and HEEC-Cr(VI) cells. Scale bars as shown. (d-f) The proliferation of HEECs and HEEC-Cr(VI) cells was assessed using the EdU incorporation (d), CCK-8 (e), and plate colony formation assays (f). Scale bars in (d) as indicated. (g) A sphere formation assay was applied to evaluate the stemness of HEECs and HEEC-Cr(VI) cells. Representative images with a scale bar and the quantification as displayed. (h) The protein levels of c-Myc and SOX-2 were detected using western blot. β-Actin was used as a loading control. (i-k) BALB/c nude mice (n=7) were subcutaneously xeno-grafted with HEECs or HEEC-Cr(VI) cells for 19 days. Tumor growth curve (i), the image of xenografts (j), and quantification for tumor weights (k) as shown. All data for statistical analysis are displayed as means ± SD. Statistical significance was determined by performing an unpaired t-test in (c, d, f, g, k) or a two-way ANOVA in (e, i).

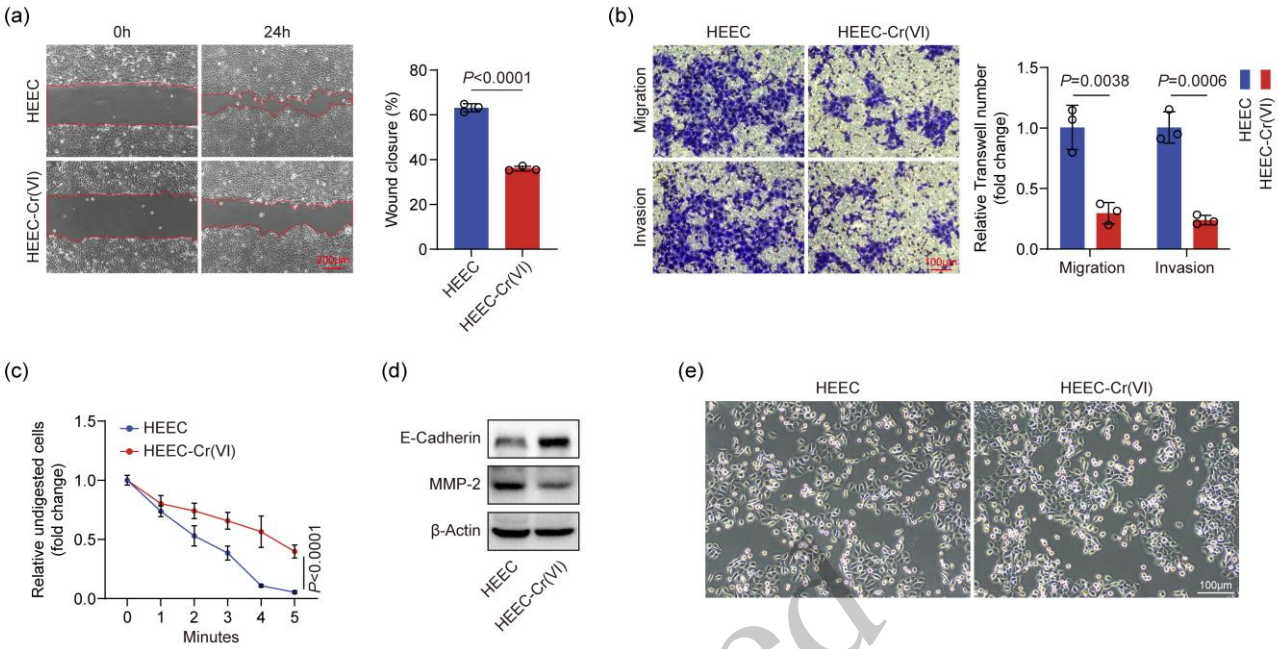

Fig.2. HEEC-Cr(VI) cells exhibit weakened cell motility and enhanced cell adhesion.
(a) Wound healing assays were performed for the migration capacity of HEEC and HEEC-Cr(VI) cells. (b) The ability of cell migration and invasion was evaluated using a transwell assay. The scale bar (red line) in the representative image is 100 μm. (c) HEECs and HEEC-Cr(VI) cells were subjected to the digestion of trypsin for the indicated time. Then, adherent cells were counted. (d) Western blot analysis was applied to detect the protein levels of E-Cadherin and MMP-2 in HEECs and HEEC-Cr(VI) cells. β-Actin protein was applied as a loading control. (e) The morphological characteristics of HEECs and HEEC-Cr(VI) cells under an inverted microscope. Scale bars as shown. All data for statistical analysis are presented as means ± SD. An unpaired *t*-test was used to determine the statistical significance in (a, b), while the two-way ANOVA was used in (c).

Unedited

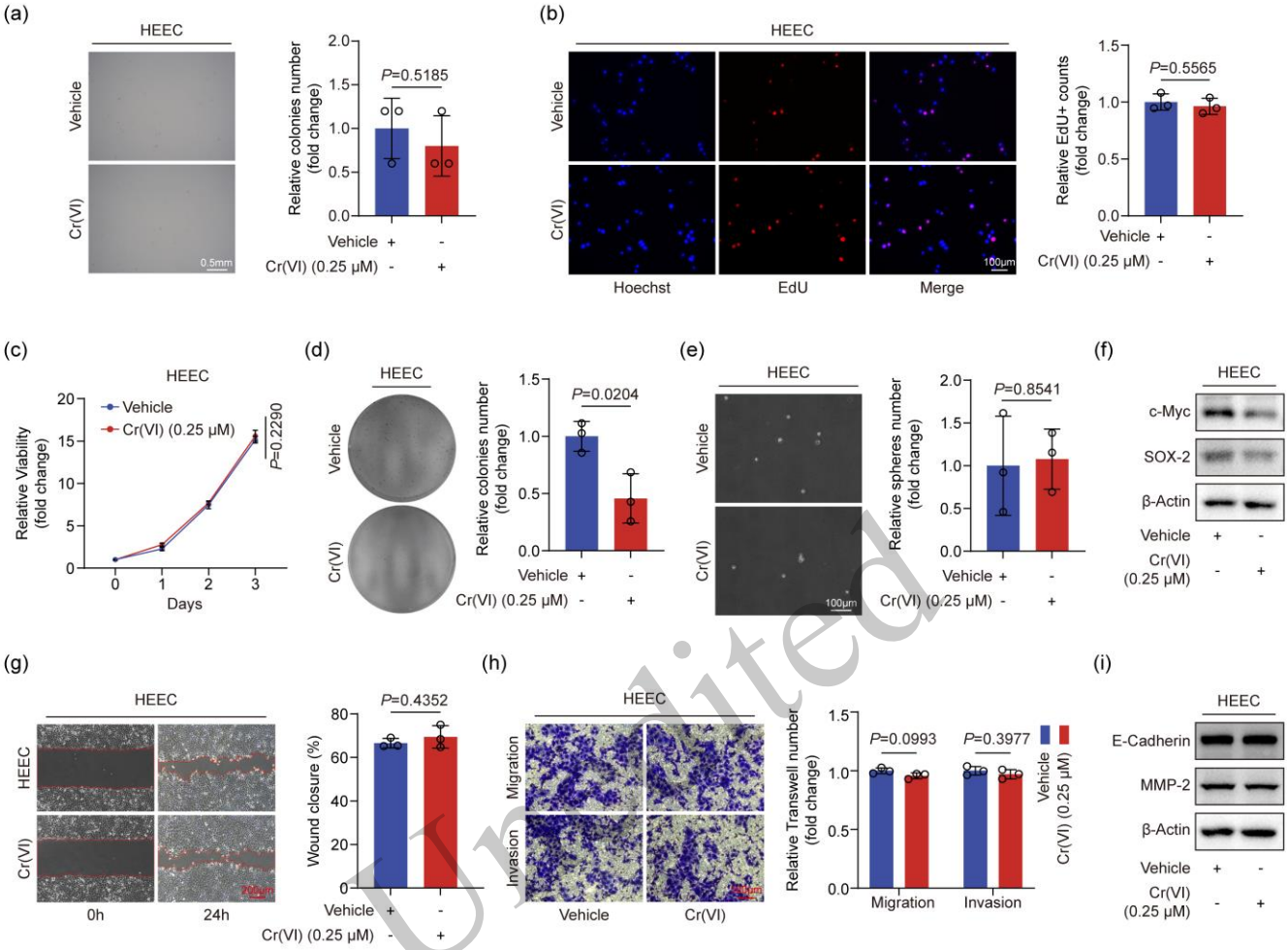

Unedited

Fig.3. Acute exposure to Cr(VI) failed to confer HEECs with the characteristics of HEEC-Cr(VI) cells.
(a) HEECs were treated with Cr(VI) (0.25 μM) or vehicle control for 48 hours, followed by soft agar colony formation assays to assess cell anchorage-independent growth. Scale bars as displayed. (b-d) The EdU incorporation (b), CCK-8 (c), and plate colony formation assays (d) were performed to detect the proliferative capacity of HEECs with or without exposure to Cr(VI) (0.25 μM) for 48 hours. Scale bars in (b) as shown. (e) HEECs were treated with Cr(VI) (0.25 μM) for 48 hours or not, followed by a sphere formation assay to evaluate the stemness. Representative images with a scale bar and the quantification as indicated. (f) Western blot analysis was performed to determine SOX-2 and c-Myc protein levels in HEECs treated with Cr(VI) (0.25 μM) for 48 hours or not. Loading control for western blot refers to β-Actin protein levels. (g, h) The wound healing (g) and transwell assays (h) were used to evaluate the migration and invasion of HEECs with or without acute exposure (48 hours) to Cr(VI) (0.25 μM). The scale bar (red line) in (h) indicates 100 μm. (i) E-Cadherin and MMP-2 proteins were detected in HEECs with acute exposure (48 hours) to Cr(VI) (0.25 μM) or not using western blot. β-Actin protein levels were applied for loading control. The data for statistical analysis are indicated as means ± SD. Statistical significance was identified by applying an unpaired *t*-test in (a, b, d, e, g, h) or the two-way ANOVA in (c).

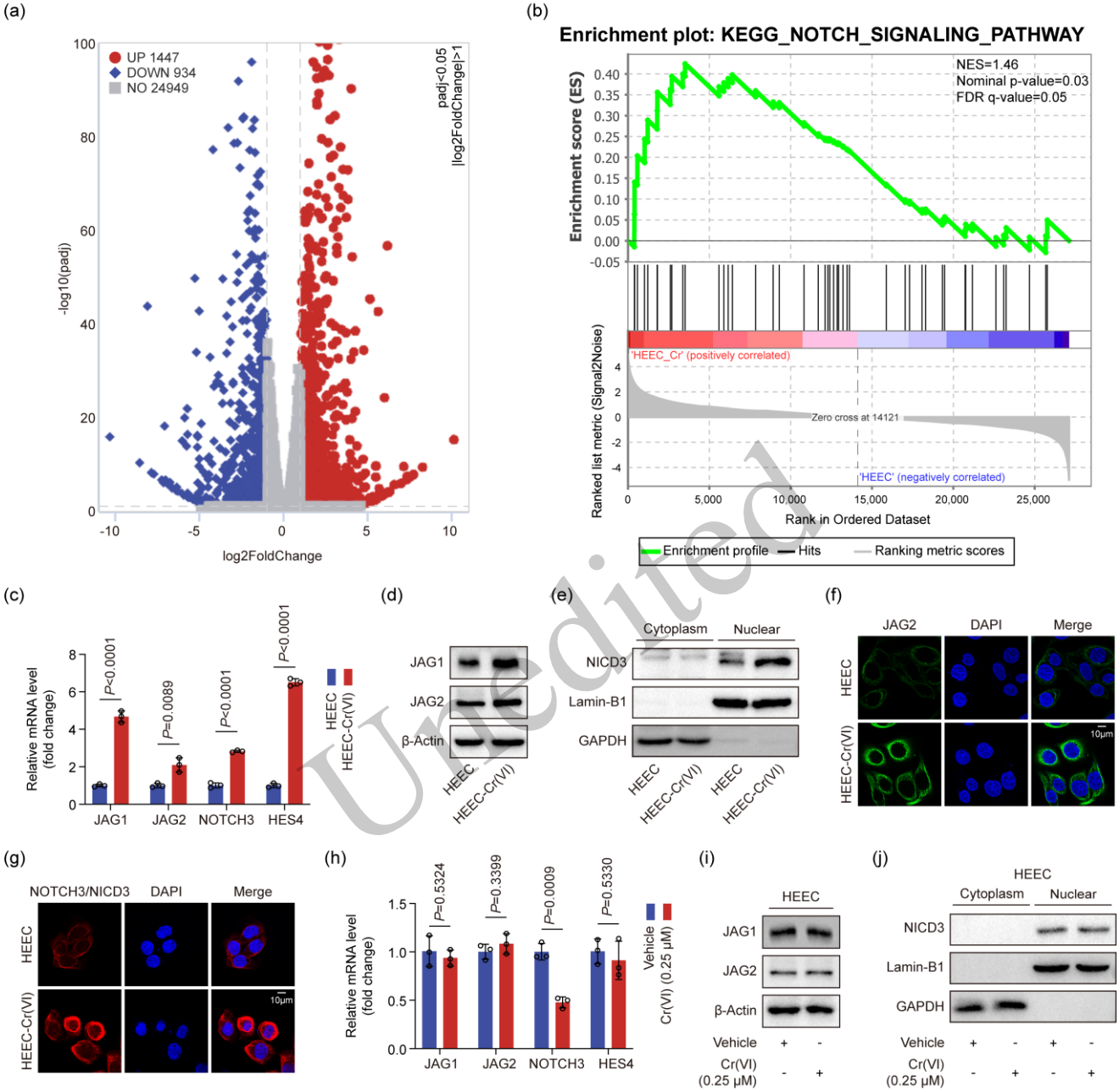

Unedited

Fig. 4. The Notch signaling pathway is aberrantly activated in HEEC-Cr(VI) cells.
(a) The volcano diagram was applied to show differentially expressed genes (DEGs) between HEEC-Cr(VI) and HEECs according to the data from RNA-Seq. HEECs were used as the control group. (b) Gene Set Enrichment Analysis (GSEA) was conducted to evaluate the status of the Notch signaling pathway in HEEC-Cr(VI) cells. (c) The mRNA levels of JAG1, JAG2, NOTCH3, and HES4 in HEECs and HEEC-Cr(VI) cells were detected using RT-qPCR. GAPDH mRNA levels were used as an internal control. (d) JAG1 and JAG2 protein levels in HEECs and HEEC-Cr(VI) cells were determined by western blot analysis. (e) Cytoplasmic and nuclear proteins from HEECs or HEEC-Cr(VI) cells were, respectively, extracted and then subjected to western blot for detecting active truncate of NOTCH3 protein (NICD3) levels. (f, g) Subcellular locations of JAG2 (f) and NOTCH3 proteins (g) were identified using IF assays. Scale bar as indicated. (h-j) HEECs were treated with 0.25 μM of Cr(VI) or vehicle control for 48 hours, followed by RT-qPCR to detect JAG1, JAG2, NOTCH3, and HES4 mRNA levels (h) and by western blot to evaluate protein levels of JAG1, JAG2 (i), and NICD3 (j). The data in (c, h) are indicated as means ± SD, and the statistical significance for the difference was identified by using an unpaired *t*-test.

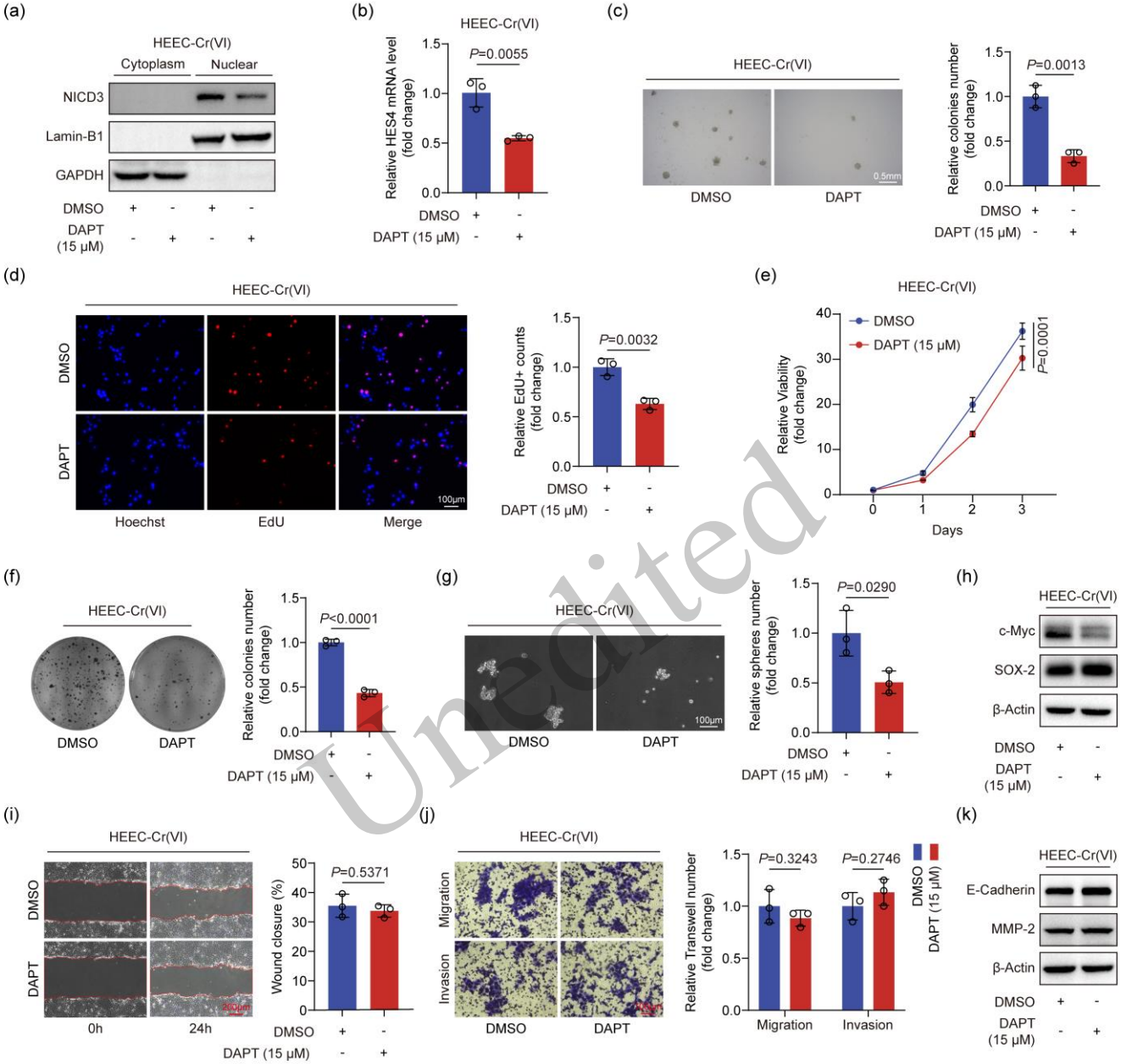

Unedited

Fig.5. Blockage of the Notch signaling pathway impairs the malignant proliferation and stemness of HEEC-Cr(VI) cells. (a, b) HEEC-Cr(VI) cells were treated with DAPT (15 μM), a potent inhibitor against the Notch signaling pathway, or vehicle control for 48 hours and then subjected to western blot to assess protein levels of active NOTCH3 protein truncate (NICD3) (a) and RT-qPCR to determine HES4 mRNA levels (b). Lamin-B1 and GAPDH protein were respectively used as a loading control for the nucleus and cytoplasmic protein lysate. GAPDH mRNA levels were applied as an internal control for RT-qPCR. (c) The anchorage-independent growth of HEEC-Cr(VI) cells in DAPT (15 μM) or vehicle control groups was evaluated by soft agar colony formation assays. The treatment of DAPT (15 μM) continued throughout the whole process of experiments (3 weeks). Scale bar as indicated. (d, e) HEEC-Cr(VI) cells were treated with DAPT (15 μM) or vehicle control for 48 hours. Then, the proliferation of treated cells was evaluated by the EdU incorporation (d) and CCK-8 (e). (f) Plate colony formation assays were applied to evaluate the proliferation of HEEC-Cr(VI) cells treated with DAPT (15 μM) or vehicle control. DAPT (15 μM) treatment continued throughout the whole process of plate colony formation assays (2 weeks). (g) A sphere formation assay was used to assess the stemness of HEEC-Cr(VI) cells treated with DAPT (15 μM) or vehicle for the whole experimental process (2 weeks). Representative images with a scale bar and the quantification as shown. (h) HEEC-Cr(VI) cells were treated with DAPT (15 μM) or

vehicle for 48 hours, then subjected to western blot analysis to detect SOX-2 and c-Myc protein levels. β-Actin protein was applied as a loading control. (i, j) After treating HEEC-Cr(VI) cells with DAPT (15 μM) or vehicle for 48 hours, the wound healing (i) and transwell assays (j) were applied to assess cell migration and invasion. The scale bar (red line) in (j) indicates 100 μm. (k) Western blot analysis was used to detect the protein levels of E-Cadherin and MMP-2 in HEEC-Cr(VI) cells treated with DAPT (15 μM) or vehicle for 48 hours. All data for statistical analysis are displayed as means ± SD. An unpaired *t*-test was applied to identify the statistical significance (b, c, d, f, g, i, j) while the two-way ANOVA was used in (e).

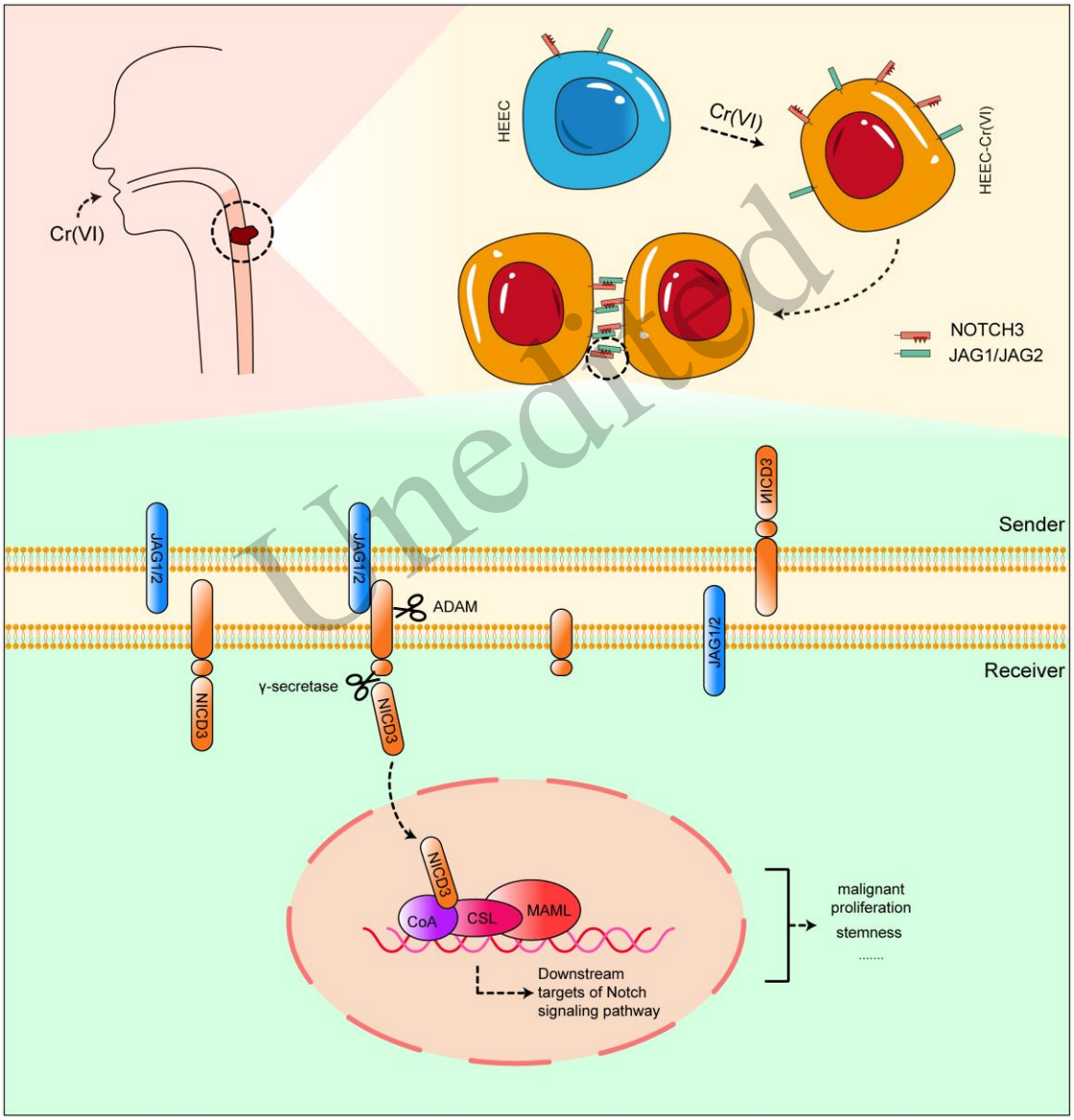

Unedited

Fig.6. Schematic diagram elucidating the regulatory mechanism underlying the Cr(VI)-induced esophageal tumorigenesis.

References

No author listed, 2022. Guidelines for drinking-water quality: Fourth edition incorporating the first and second addenda. Geneva,

Abnet CC, Arnold M, Wei WQ, 2018. Epidemiology of esophageal squamous cell carcinoma. Gastroenterology, 154(2):360-373. https://doi.org/10.1053/j.gastro.2017.08.023

Amer MH, El-Yazigi A, Hannan MA, et al., 1990. Water contamination and esophageal cancer at gassim region, saudi arabia. Gastroenterology, 98(5 Pt 1):1141-1147. https://doi.org/10.1016/0016-5085(90)90326-v

An L, Zheng R, Zeng H, et al., 2023. The survival of esophageal cancer by subtype in china with comparison to the united states. Int J Cancer, 152(2):151-161. https://doi.org/10.1002/ijc.34232

Aponte PM, Caicedo A, 2017. Stemness in cancer: Stem cells, cancer stem cells, and their microenvironment. Stem Cells Int, 2017:5619472. https://doi.org/10.1155/2017/5619472

Brabletz S, Schuhwerk H, Brabletz T, et al., 2021. Dynamic emt: A multi-tool for tumor progression. EMBO J, 40(18):e108647. https://doi.org/10.15252/embj.2021108647

Cai J, Qiao Y, Chen L, et al., 2023. Regulation of the notch signaling pathway by natural products for cancer therapy. J Nutr Biochem, 123:109483. https://doi.org/10.1016/j.jnutbio.2023.109483

Chen QY, Murphy A, Sun H, et al., 2019. Molecular and epigenetic mechanisms of cr(vi)-induced carcinogenesis. Toxicol Appl Pharmacol, 377:114636. https://doi.org/10.1016/j.taap.2019.114636

Chrysochoou M, Theologou E, Bompoti N, et al., 2016. Occurrence, origin and transformation processes of geogenic chromium in soils and sediments. 2:224-235.

Fantoni D, Brozzo G, Canepa M, et al., 2002. Natural hexavalent chromium in groundwaters interacting with ophiolitic rocks. 42:871-882.

Freedman VH, Shin SI, 1974. Cellular tumorigenicity in nude mice: Correlation with cell growth in semi-solid medium. Cell, 3(4):355-359. https://doi.org/10.1016/0092-8674(74)90050-6

Goldman MJ, Craft B, Hastie M, et al., 2020. Visualizing and interpreting cancer genomics data via the xena platform. Nat Biotechnol, 38(6):675-678. https://doi.org/10.1038/s41587-020-0546-8

Hashemian M, Murphy G, Etemadi A, et al., 2017. Toenail mineral concentration and risk of esophageal squamous cell carcinoma, results from the golestan cohort study. Cancer Med, 6(12):3052-3059. https://doi.org/10.1002/cam4.1247

Hsieh MH, Choe JH, Gadhvi J, et al., 2019. P63 and sox2 dictate glucose reliance and metabolic vulnerabilities in squamous cell carcinomas. Cell Rep, 28(7):1860-1878 e1869. https://doi.org/10.1016/j.celrep.2019.07.027

Hu G, Li P, Li Y, et al., 2016. Methylation levels of p16 and tp53 that are involved in DNA strand breakage of 16hbe cells treated by hexavalent chromium. Toxicol Lett, 249:15-21. https://doi.org/10.1016/j.toxlet.2016.03.003

Hu G, Li P, Cui X, et al., 2018. Cr(vi)-induced methylation and down-regulation of DNA repair genes and its association with markers of genetic damage in workers and 16hbe cells. Environ Pollut, 238:833-843. https://doi.org/10.1016/j.envpol.2018.03.046

Islam S, Kamila S, Chattopadhyay A, 2022. Toxic and carcinogenic effects of hexavalent chromium in mammalian cells in vivo and in vitro: A recent update. J Environ Sci Health C Toxicol Carcinog, 40(3-4):282-315. https://doi.org/10.1080/26896583.2022.2158675

Iyer M, Anand U, Thiruvenkataswamy S, et al., 2023. A review of chromium (cr) epigenetic toxicity and health hazards. Sci Total Environ, 882:163483. https://doi.org/10.1016/j.scitotenv.2023.163483

Jiang A, Gong L, Ding H, et al., 2021. Cancer mortality and long-term environmental exposure of cadmium in contaminated community based on a third retrospective cause of death investigation of residents living in the guangdong province from 2004 to 2005. Biol Trace Elem Res, 199(12):4504-4515. https://doi.org/10.1007/s12011-021-02599-0

Jing N, Gao WQ, Fang YX, 2021. Regulation of formation, stemness and therapeutic resistance of cancer stem cells. Front Cell Dev Biol, 9:641498. https://doi.org/10.3389/fcell.2021.641498

Kopan R, Ilagan MX, 2009. The canonical notch signaling pathway: Unfolding the activation mechanism. Cell, 137(2):216-233. https://doi.org/10.1016/j.cell.2009.03.045

Lee CP, Lee YH, Lian IB, et al., 2016. Increased prevalence of esophageal cancer in areas with high levels of nickel in farm soils. J Cancer, 7(12):1724-1730. https://doi.org/10.7150/jca.15441

Li P, Zhang X, Murphy AJ, et al., 2021a. Downregulation of hedgehog-interacting protein (hhip) contributes to hexavalent chromium-induced malignant transformation of human bronchial epithelial cells. Carcinogenesis, 42(1):136-147. https://doi.org/10.1093/carcin/bgaa085

Li X, Yan X, Wang Y, et al., 2023. The notch signaling pathway: A potential target for cancer immunotherapy. J Hematol Oncol, 16(1):45. https://doi.org/10.1186/s13045-023-01439-z

Li Y, Li Y, Chen X, 2021b. Notch and esophageal squamous cell carcinoma. Adv Exp Med Biol, 1287:59-68. https://doi.org/10.1007/978-3-030-55031-8_5

Morgan E, Soerjomataram I, Rumgay H, et al., 2022. The global landscape of esophageal squamous cell carcinoma and esophageal adenocarcinoma incidence and mortality in 2020 and projections to 2040: New estimates from globocan 2020. Gastroenterology, 163(3):649-658 e642. https://doi.org/10.1053/j.gastro.2022.05.054

National Toxicology P, 2008. Toxicology and carcinogenesis studies of sodium dichromate dihydrate (cas no. 7789-12-0) in f344/n rats and b6c3f1 mice (drinking water studies). Natl Toxicol Program Tech Rep Ser, (546):1-192.

Natsuizaka M, Whelan KA, Kagawa S, et al., 2017. Interplay between notch1 and notch3 promotes emt and tumor initiation in squamous cell carcinoma. Nat Commun, 8(1):1758. https://doi.org/10.1038/s41467-017-01500-9

Unedited

Nowell CS, Radtke F, 2017. Notch as a tumour suppressor. Nat Rev Cancer, 17(3):145-159. https://doi.org/10.1038/nrc.2016.145
Nozadi F, Azadi N, Mansouri B, et al., 2021. Association between trace element concentrations in cancerous and non-cancerous tissues with the risk of gastrointestinal cancers in eastern iran. Environ Sci Pollut Res Int, 28(44):62530-62540. https://doi.org/10.1007/s11356-021-15224-3
Nunez O, Fernandez-Navarro P, Martin-Mendez I, et al., 2016. Arsenic and chromium topsoil levels and cancer mortality in spain. Environ Sci Pollut Res Int, 23(17):17664-17675. https://doi.org/10.1007/s11356-016-6806-y
Ranganathan P, Weaver KL, Capobianco AJ, 2011. Notch signalling in solid tumours: A little bit of everything but not all the time. Nat Rev Cancer, 11(5):338-351. https://doi.org/10.1038/nrc3035
Sawangarun W, Mandasari M, Aida J, et al., 2018. Loss of notch1 predisposes oro-esophageal epithelium to tumorigenesis. Exp Cell Res, 372(2):129-140. https://doi.org/10.1016/j.yexcr.2018.09.019
Schneider CA, Rasband WS, Eliceiri KW, 2012. Nih image to imagej: 25 years of image analysis. Nature Methods, 9(7):671-675.
Sheng F, Chen KX, Liu J, et al., 2021. Chromium (vi) promotes emt by regulating flna in blca. Environ Toxicol, 36(8):1694-1701. https://doi.org/10.1002/tox.23165
Shin SI, Freedman VH, Risser R, et al., 1975. Tumorigenicity of virus-transformed cells in nude mice is correlated specifically with anchorage independent growth in vitro. Proc Natl Acad Sci U S A, 72(11):4435-4439. https://doi.org/10.1073/pnas.72.11.4435
Sohrabi M, Nikkhah M, Sohrabi M, et al., 2021. Evaluating tissue levels of the eight trace elements and heavy metals among esophagus and gastric cancer patients: A comparison between cancerous and non-cancerous tissues. J Trace Elem Med Biol, 68:126761. https://doi.org/10.1016/j.jtemb.2021.126761
Stout MD, Herbert RA, Kissling GE, et al., 2009. Hexavalent chromium is carcinogenic to f344/n rats and b6c3f1 mice after chronic oral exposure. Environ Health Perspect, 117(5):716-722. https://doi.org/10.1289/ehp.0800208
Subramanian A, Tamayo P, Mootha VK, et al., 2005. Gene set enrichment analysis: A knowledge-based approach for interpreting genome-wide expression profiles. Proc Natl Acad Sci U S A, 102(43):15545-15550. https://doi.org/10.1073/pnas.0506580102
Sun H, Clancy HA, Kluz T, et al., 2011. Comparison of gene expression profiles in chromate transformed beas-2b cells. PLoS One, 6(3):e17982. https://doi.org/10.1371/journal.pone.0017982
Sun H, Brocato J, Costa M, 2015. Oral chromium exposure and toxicity. Curr Environ Health Rep, 2(3):295-303. https://doi.org/10.1007/s40572-015-0054-z
Sun W, Gaykalova DA, Ochs MF, et al., 2014. Activation of the notch pathway in head and neck cancer. Cancer Res, 74(4):1091-1104. https://doi.org/10.1158/0008-5472.CAN-13-1259
Sung H, Ferlay J, Siegel RL, et al., 2021. Global cancer statistics 2020: Globocan estimates of incidence and mortality worldwide for 36 cancers in 185 countries. CA Cancer J Clin, 71(3):209-249. https://doi.org/10.3322/caac.21660
Tang D, Chen M, Huang X, et al., 2023. Srplot: A free online platform for data visualization and graphing. PLoS One, 18(11):e0294236. https://doi.org/10.1371/journal.pone.0294236
You BH, Yoon JH, Kang H, et al., 2019. Heres, a lncrna that regulates canonical and noncanonical wnt signaling pathways via interaction with ezh2. Proc Natl Acad Sci U S A, 116(49):24620-24629. https://doi.org/10.1073/pnas.1912126116
Zeidler-Erdely PC, Falcone LM, Antonini JM, et al., 2020. Tumorigenic response in lung tumor susceptible a/j mice after sub-chronic exposure to calcium chromate or iron (iii) oxide. Toxicol Lett, 334:60-65. https://doi.org/10.1016/j.toxlet.2020.09.012
Zhang C, Cai K, Feng Q, et al., 2019. Chromium(vi) promotes cell migration through targeting epithelial-mesenchymal transition in prostate cancer. Toxicol Lett, 300:10-17. https://doi.org/10.1016/j.toxlet.2018.10.012
Zhang Z, Cao H, Song N, et al., 2020. Long-term hexavalent chromium exposure facilitates colorectal cancer in mice associated with changes in gut microbiota composition. Food Chem Toxicol, 138:111237. https://doi.org/10.1016/j.fct.2020.111237
Zhong R, Bao R, Faber PW, et al., 2015. Notch1 activation or loss promotes hpv-induced oral tumorigenesis. Cancer Res, 75(18):3958-3969. https://doi.org/10.1158/0008-5472.CAN-15-0199
Zhou B, Lin W, Long Y, et al., 2022. Notch signaling pathway: Architecture, disease, and therapeutics. Signal Transduct Target Ther, 7(1):95. https://doi.org/10.1038/s41392-022-00934-y

Supplementary information:
Tables S1 and S2; Figs. S1-9; Raw data for western blot.

Unedited